Smectic blue phases: Layered systems with high intrinsic curvature

B. A. DiDonna and Randall D. Kamien*
Department of Physics and Astronomy, University of Pennsylvania, Philadelphia, Pennsylvania 19104-6396, USA
(Received 7 July 2003; published 13 October 2003)

We report on a construction for smectic blue phases, which have quasi-long-range smectic translational order as well as three-dimensional crystalline order. Our proposed structures fill space by adding layers on top of a minimal surface, introducing either curvature or edge defects as necessary. We find that for the right range of material parameters, the favorable saddle-splay energy of these structures can stabilize them against uniform layered structures. We also consider the nature of curvature frustration between mean curvature and saddle splay.

DOI: 10.1103/PhysRevE.68.041703 PACS number(s): 61.30.Mp, 61.30.Jf, 02.40.−k

I. INTRODUCTION

Topological defects and liquid crystal phases are hopelessly intertwined. Historically, the nematic phase derived it's name from the observation of long disclination lines. In some liquid crystal phases, such as the twist-grain-boundary (TGB) phases and blue phases, these defects are not simply artifact or nuisance, but instead act to stabilize the director field configuration. While the TGB phases have smectic order, the blue phases have purely nematiclike order created by a long range, triply periodic lattice of line defects. Two of the nematic blue phases possess cubic symmetry (BP1 and BP2), while the third (BP3) is thought to be an isotropic melt of double-twist cylinders [1,2]. Recently, new phases of matter have been identified that possess the quasi-long-range translational order of smectics [3] in addition to three-dimensional orientational order. These phases, dubbed the ''smectic blue phases,'' have been observed for molecules in the chiral series FH/FH/HH-*n*BTMHC, where *n* is the aliphatic chain length. Three distinct smectic blue phases have been observed near the isotropic transition of these compounds: $BP_{SmA}1$ has cubic symmetry, $BP_{Sm}2$ has orthorhombic symmetry, and $BP_{Sm}3$ is isotropic [4]. The precise physical properties of these materials have been the study of intense investigation in recent years [4–7].

In general, since smectic order is incompatible with cubic symmetry, it is expected that any triply periodic crystalline structure must include smectic dislocations as well as disclinations. However, attempts to construct smectic double-twist cylinders [8] and assemble them into traditional blue phase structures [9] present a variety of difficulties, most notably a disagreement with precise experimental details [6]. In previous work [10] we proposed a model for the smectic blue phases. Our construction filled space with concentric minimal surfaces wrapping a lattice of intersecting line defects. We found that when the saddle-splay constant was large enough, these new structures were stable. Though the new materials were chiral, our construction did not rely on macroscopic chirality as in the traditional blue phases. Instead, the smectic compression and bending energies set the length scale of our solutions.

Here, we refine our earlier model through variations on the original construction. We find that by allowing edge dislocations our phase is stabilized for even small (negative) values of the saddle-splay constant K_{24}. This paper is organized as follows. In Sec. II we discuss the rotationally invariant energetics of layered systems and derive detailed equations for the geometric frustration between curvature and uniform layer spacing. Next, in Sec. III, we calculate the energy and stability of likely smectic structures based on our original construction [10]. To supplement our analytical calculations, we present the results of simplified numerical solutions for the three-dimensional smectic structure, which explore relaxation of the smectic layers away from our constructions. In Sec. IV we present a construction for filling space based on uniform layer spacing away from a minimal surface. First we derive formulas for the evolution of curvature fields in layered space and then we employ the Weierstraß analytic representation of minimal surfaces to calculate the energies for our proposed phase. We complete our description by calculating the core energy and argue that tilt-grain boundaries form at the cores of our structures. Numerics are also presented for this construction. Finally, in Sec. V we calculate the Fourier transform of the smectic density and compare it with experimental x-ray results. In Appendix A we derive curvature evolution equations in curved space and in Appendix B we review the Weierstraß representation for completeness.

II. ENERGETICS AND CONSTRUCTION

The similarity between the crystal structures and phase diagrams of the nematic and smectic blue phases suggests that, like the nematic blue phases, the smectic phases are stabilized through saddle splay. The key to our construction is the observation that saddle splay and Gaussian curvature are identical [11] for layered systems with uniform spacing. The saddle-splay energy of a unit director field **N** is [9]

$$F_{SS}=K_{24}\int d^3x\,\boldsymbol{\nabla}\cdot[(\mathbf{N}\cdot\boldsymbol{\nabla})\mathbf{N}-\mathbf{N}(\boldsymbol{\nabla}\cdot\mathbf{N})], \qquad (1)$$

where K_{24} is a Frank constant. In a layered system, we can rewrite the expression for F_{SS} in a more useful form by employing a local coordinate system where one direction is

*Electronic address: kamien@physics.upenn.edu

parallel to the local layer normal **N**. This frame is appropriate in the limit where the nematic director and the layer normal are locked. Then Eq. (1) becomes

$$F_{\mathrm{SS}} = -2K_{24}\int dn \int dx\, dy \sqrt{g_n(x,y)}\, a_n(x,y) K_n(x,y), \tag{2}$$

where n is the Lagrangian coordinate which labels the layers, $a_n(x,y)$ is the local layer spacing at (x,y), K_n is the Gaussian curvature of the nth surface, and g_n is the determinant of the two-dimensional, induced, surface metric. In the special case that $a_n(x,y)$ is constant, the integral becomes purely topological: a consequence of the Gauss-Bonnet theorem [11] is that for a surface of genus g, the integrated Gaussian curvature is $4\pi(1-g)$. Since $g>0$ for any infinite surface [12], F_{SS} is large and negative when $K_{24}<0$ and the unit cells contain surfaces with large genus, i.e., many handles and holes. Note that here, the saddle splay is a measure of the layer normals and not the nematic director. When the nematic director follows the layer normal these are, of course, equivalent. As discussed in Ref. [10], in type-II smectics it is possible for the saddle splay of the director field to differ in its precise numerical value from the saddle splay in the layers.

In addition to the saddle splay, we must include the rotationally invariant bulk free energy

$$F_{\mathrm{Sm}} = \int d^3x \left\{ \frac{B}{4}[(\boldsymbol{\nabla}\Phi)^2 - 1]^2 + 2K_1 \mathbf{H}^2 \right\}, \tag{3}$$

where the smectic density is $\rho \propto \cos(2\pi\Phi/a_0)$, $\Phi(x,y,z)$ is a phase field, a_0 is the layer spacing, B is the compression modulus, K_1 is the bend modulus, and $H = \frac{1}{2}\boldsymbol{\nabla}\cdot\mathbf{N}$ is the mean curvature of the layers. If the two principle curvatures are κ_1 and κ_2, $K_G = \kappa_1\kappa_2$, and $H = (\kappa_1+\kappa_2)/2$ [11].

Together, Eqs. (2) and (3) favor configurations with uniform layer spacing, low mean curvature, and high Gaussian curvature. However, there is an unavoidable geometric frustration between these three terms. When a surface is displaced along its normal by δa, the changes in the metric and curvature tensors are [13]

$$\delta g_{ij} = 2\kappa_{ij}\delta a,$$

$$\delta\kappa_{ij} = -\nabla_i\nabla_j\delta a + \kappa_{ik}\kappa^k_j\delta a. \tag{4}$$

It is straightforward to find the variation in the mean and Gaussian curvatures:

$$\delta H = [K_G - 2H^2]\delta a - \tfrac{1}{2}g^{ij}\nabla_i\nabla_j\delta a,$$

$$\delta K_G = -2K_G H\delta a - \tilde{\kappa}^{ij}\nabla_i\nabla_j\delta a, \tag{5}$$

where ∇_i is the covariant derivative on the surface and $\tilde{\kappa}^{ij} \equiv \epsilon^{ik}\epsilon^{jl}\kappa_{kl}/|g|$, where ϵ^{ij} is the completely antisymmetric tensor.

If we impose smectic order, then a may also be interpreted as the normal distance between adjacent layers. When the spacing is uniform, $\mathbf{N}\cdot\boldsymbol{\nabla}\Phi$ is constant and $\nabla_i\delta a = 0$. In this case, the first result in Eq. (5) implies $\partial H/\partial a = 0$ if and only if the principal curvatures κ_i satisfy

$$\kappa_1^2 + \kappa_2^2 = 0, \tag{6}$$

i.e., $\kappa_1 = \kappa_2 = 0$. Thus if $K_G \neq 0$ and the layer spacing is uniform, then $\partial H/\partial a \neq 0$; Gaussian curvature leads to mean curvature.

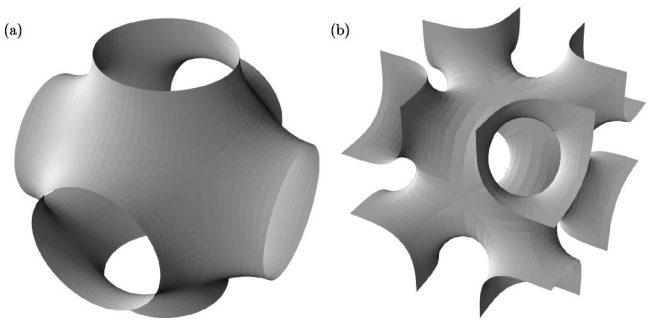

FIG. 1. Minimal surface repeat units: (a) P surface, (b) I-Wp surface.

For uniform spacing the evolution equations become particularly simple. The variation δa is constant and the equations can be integrated:

$$H(a) = \frac{H + aK_G}{1 + 2aH + a^2K_G},$$

$$K_G(a) = \frac{K_G}{1 + 2aH + a^2K_G}. \tag{7}$$

Alternatively, this evolution follows from the observation that if the principle radii of curvature are $R_1 = \kappa_1^{-1}$ and $R_2 = \kappa_2^{-1}$ for one surface then the radii for the surface displaced by a along the local normal are $R_i(a) = R_i + a$. Thus, in layered systems, Gaussian curvature in one region implies mean curvature in another. Furthermore, as we continue to develop the initial layer, there will be a curvature singularity at a distance $a = (-H \pm \sqrt{H^2 - K_G})/K_G$ normal to the original surface, i.e., at one of the radii of curvature.

With these geometric constraints in mind, we construct a solution which strikes a promising balance between mean and Gaussian curvatures. To do this, we build the smectic order by adding layers on top of a triply periodic minimal surface. By starting with a minimal surface, we bias our structures to have a low total mean curvature energy. In Ref. [10], we based our construction on the Schwartz P surface, pictured in Fig. 1(a). In this paper, we present calculations for both the P surface and Schoen's I-Wp surface, pictured in Fig. 1(b), a surface with a larger genus and thus a more negative saddle splay energy. The P surface is an archetypal triply periodic minimal surface and will provide a basis of comparison with earlier results, while the I-Wp surface shares the symmetries of experimental $\mathrm{Sm}_{\mathrm{BP}}$ systems [6]; the latter will also prove to be more stable than the P surface. We will consider two variations of this construction: in the first we will allow the layer spacing to vary, while in the second

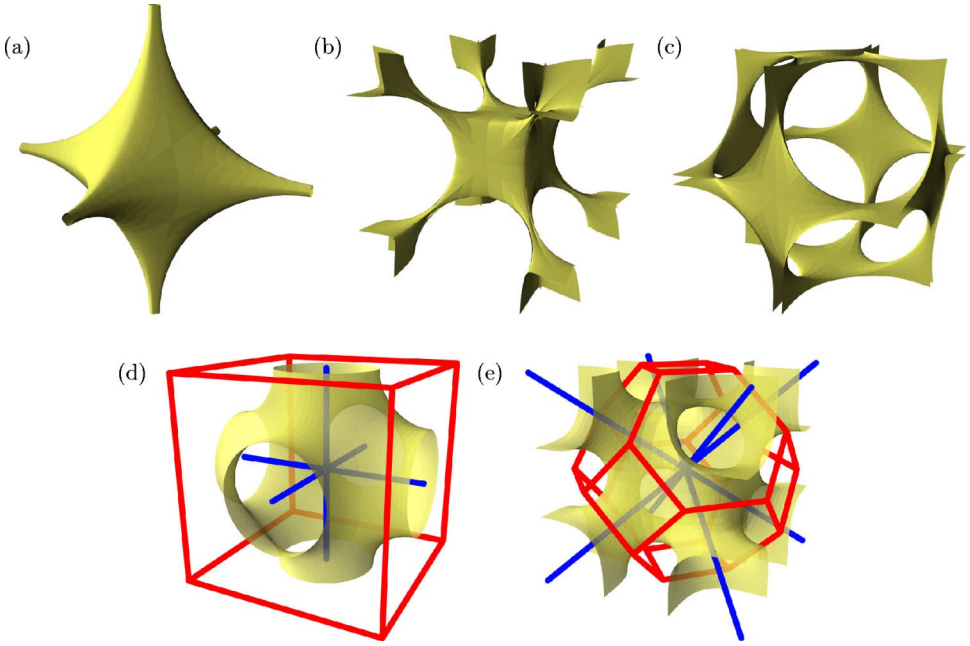

FIG. 2. (Color online) In (a) we show the P surface translated inward until self-intersection. In (b) and (c), the I-Wp surface is translated inward and outward, respectively. Figures (d) and (e) indicate the line defect structure for our construction, based on skeletal graphs.

we do not. In the former we find that the cores are composed of topological line defects, while in the latter we find that domain walls form in the relatively larger cores.

III. SMALL-CORE MODEL: SELF-SIMILAR LAYERING

A. Geometric construction

In this section we consider space-filling, layered structures in which each layer is continuous and every layer has the same global topology. We begin with a minimal surface and devise an explicit construction for filling the region away from that surface. We note that our bulk phase must contain line defects, since at some point the curvature will diverge, as is implied by Eqs. (7). By design, the layers immediately surrounding these line defects will have the same topology as the original surface. Therefore, the next logical step in our construction is to guess the optimal line defect structure.

Besides selecting the correct topology, we should choose a defect complexion that minimizes the compression energy in the region between the minimal surface and the defects: it should, as much as possible, be equidistant from the minimal surface at each point. Thus, an ansatz for the optimal structure is generated by uniformly translating the minimal surface along its normal until it self-intersects, as shown in Fig. 2. The line defects will be disclinations of charge $+1$ or $+1/2$. In the case of charge $+1$ disclinations the layers immediately surrounding them are tight cylinders. From Fig. 2(a), we see that the defects in the P surface are all $+1$. From Figs. 2(b) and 2(c), we see that the defects inside the I-Wp surface should have charge $+1$, but that outside, the translated layer approaches itself in a plane rather than on a line and so the disclination charge is $+1/2$. Figures 2(d) and 2(e) show our proposed defect structures. For the defect structure outside the I-Wp surface, the location of the intersection of defect lines is a variable chosen to minimize the total compression energy. It should be noted that in the case where all defects happen to be charge $+1$, our requirements of topology and equal spacing are exactly those best satisfied by the skeletal graph of the minimal surface [14]. We take the core region around the defect lines to have a radius of order a_0, the smectic layer spacing. We model the core as a melted region of smectic with a free energy arising from the condensation energy.

Finally, we fill the region between minimal surface and defects with continuous layers. We desire to have as little mean curvature as possible in this region, so we fill the region with dilated copies of the original minimal surface. In order to do this, we must cut the continuous minimal surface into smaller patches: we cut the surface along lines where one surface tangent is parallel to the line defect structure, and dilate it so that it shrinks onto the vertices where defect lines meet. The separated minimal patches are connected together by cylindrical patches parallel to the line defects. When there are disclinations, we must also add some flat patches to complete the surfaces. Thus the surface tangents are continuous everywhere, and the intermediary structures transform smoothly from the minimal surface on the outside to a set of cylinders surrounding line defects on the inside. This construction fills space completely, at the expense of uniform spacing. Moreover, we have filled a large part of space with minimal surfaces and so the curvature energy is likely to be as small as possible, given the necessary curvature defects.

Figure 3 shows how this construction works for the P and I-Wp surfaces. For the P surface it is particularly simple; its construction is shown in Fig. 3(a). The line defects are along the edges of the unit cell and through the center parallel to the edges. The inside of the P surface is filled with dilated copies of the P surface repeat unit, cut at its intersection with the walls of the unit cell. The edges of the dilated P surface copies are connected to neighboring cells with cylinders. The outside of the P surface is a translated copy of the inside. The I-Wp surface is more complicated, requiring different constructions for outside and inside as well as having both $+1$ and $+1/2$ defects. Figure 3(b) illustrates the construction in-

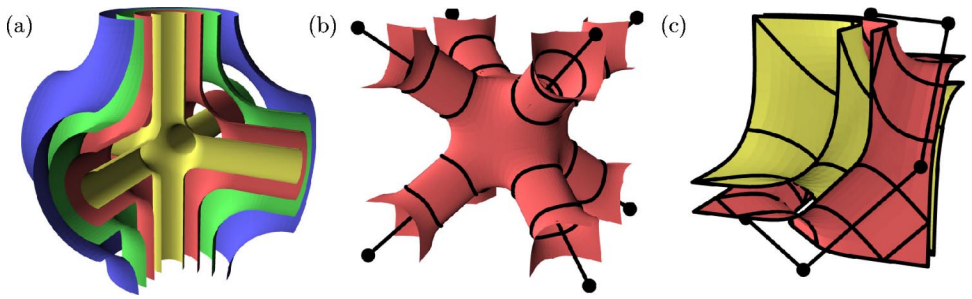

FIG. 3. (Color online) Small-core construction: (a) Partial layers inside the P surface, (b) one layer inside the I-Wp surface, and (c) partial layer around one octant outside the I-Wp surface. Each color corresponds to a different connected layer. In (b) and (c), the boundaries between minimal surface patches, cylinders, and planes are drawn in heavy black. The defect networks and vertex points are also shown.

side the I-Wp surface: the minimal surface is divided at cuts that can be smoothly attached to cylinders, then dilated towards either the center or corners of the unit cell. Figure 3(c) shows the construction outside the I-Wp surface. The surface is cut along its mirror symmetry planes, $x=y$, $x=-y$, $y=z$, etc. and $x=0$, $y=0$, and $z=0$. The resulting patches are dilated around the proper vertices in Fig. 2(e). The edges of the patches are connected together with cylinders parallel to the $+1/2$ edge defects. Finally, the free edges of the cylinder are connected together into planes.

Most of the energetics of this structure are simple to calculate; exact values are tabulated in Table I. It is instructive to derive approximate expressions for these energies so that we may quickly assess the feasibility of a given minimal surface as a starting point for our construction.

The total curvature energy comes from the contribution of the cylindrical connecting patches. Since the cylinders become progressively longer to connect the ever shrinking minimal surfaces, the bending energy of the cylinder of radius r is proportional to $(R-r)$, the length. We find that

$$F_B \approx \frac{1}{2}K_1 \int \frac{l(R-r)}{Rr}\, dr\, d\theta \approx \pi K_1 \left[\sum_{lines} l_i c_i^2\right]\left[\ln\left(\frac{\langle R\rangle}{\rho_c}\right)+\left(\frac{\rho_c}{\langle R\rangle}-1\right)\right], \qquad (8)$$

where the sum is over defect lines, l_i is the length of line i, c_i is the charge of the defect, ρ_c is the core diameter of the line defect, and $\langle R\rangle$ is the characteristic radius of the cylindrical regions. This form allows us to consider other structures without relying on the details of the fiducial surface and just on the rough length scale $\langle R \rangle$. The core energy, which is simply a condensation energy density, is approximately

$$F_{core} \approx \varepsilon \left[\sum_{lines} l_i c_i^2\right]\left(1-\frac{\rho_c}{\langle R\rangle}\right)+\varepsilon \frac{L^3}{\langle R\rangle^3}\frac{\rho_c}{\pi}, \qquad (9)$$

where ε is a line tension. The first term is the energy of the defect lines, the second is the energy of the central, melted region around vertices in the defect network. Again, we have used the characteristic radius $\langle R\rangle$ to allow us to generalize the discussion of the energetics.

Since the saddle splay is a surface term, we calculate it by integrating the strength of the nematic defects along the total length of defect core. Because the saddle splay is a total divergence, the volume integral becomes a surface integral around the defect:

$$F_{SS} = 2K_{24}\int H\, dS \approx 2\pi K_{24}\left[\sum_{lines} l_i c_i\right]\left(1-\frac{\rho_c}{\langle R\rangle}\right). \qquad (10)$$

Comparison to Eq. (8) shows that these smectic structures will favor charge $+1/2$ structures when possible. Also, for all constructions which only utilize $+1$ defects, the ratio of saddle splay to curvature energy will be approximately $2K_{24}/K_1$.

The only energy not explicitly determined by our construction is the compression energy. Though the layering is largely constrained, there is still one free variable which gives the relative dilation of consecutive surfaces. We minimize the compression energy with respect to the relative smectic layer spacing as a function of position. In the following we show how we can take advantage of the dilational symmetry of our construction to greatly simplify the exact calculation of optimal compression energy.

First we consider the compression energy in a subregion which is filled with self-similar, radially dilated patches of minimal surface. Each successive layer in this region is a

TABLE I. Smectic energy per unit cell for P and I-Wp surface constructions. The first column gives the topological genus per unit cell of the structure. F_B is the total curvature energy, F_{SS} is the saddle splay, F_{core} is energy of the defect cores, and F_C is the total compression energy.

Surface	Genus	$F_B/(K_1L)$	$F_{SS}/(\lvert K_{24}\rvert L)$	F_{core}/ε	$F_C/(BL^3)$
P	3	$6\pi[\ln(L/4\rho_c)+(4\rho_c/L-1)]$	$-12\pi(1-4\rho_c/L)$	$6(L-4\rho_c)+(64/\pi)\rho_c$	4.32×10^{-2}
I-Wp	7	$31.7[\ln(L/6.3\rho_c)+(6.3\rho_c/L-1)]$	$-68.9(1-6.3\rho_c/L)$	$9.05(L-6.1\rho_c)+72.2\rho_c$	4.85×10^{-2}

smaller version of the last, and all are centered on a common origin. Thus, if the radial coordinates of the outermost surface of this region are specified by a function $r_0(\theta,\phi)$, then the radial coordinates of any interior surface are given by $r=\zeta r_0(\theta,\phi)$, where $\zeta\in[0,1]$ parametrizes the layers. Furthermore, every point within this region has a unique value of θ, ϕ, and ζ, and conversely the values of θ, ϕ, and ζ uniquely specify the position of any point in the region, so we can use these three variables as a coordinate frame on the patch. In these coordinates, each layer is a surface of constant ζ.

In the continuum description of the smectic, the layers are surfaces of constant Φ. Since Φ is constant on each smectic layer, which is, in turn, a layer of constant ζ, it follows that $\Phi=\Phi(\zeta)$ is purely a function of ζ. Our goal is to find the form of $\Phi(\zeta)$ which minimizes the compression energy. This is nontrivial, since the compression energy goes as $\nabla\Phi$, which is not purely a function of ζ. However, we can find a combination of $|\nabla\Phi|$ times a function of angle which together is constant over each smectic layer. First we observe that

$$\Phi(\zeta)=\Phi\left(\frac{r}{r_0(\theta,\phi)}\right)\Rightarrow\frac{\partial}{\partial\zeta}\Phi(\zeta)=r_0(\theta,\phi)\frac{\partial}{\partial r}\Phi\left(\frac{r}{r_0(\theta,\phi)}\right). \tag{11}$$

Then we note that for level surfaces of Φ the field of unit normals is $\mathbf{N}=\nabla\Phi/|\nabla\Phi|$ to write

$$\begin{aligned}(\mathbf{r}\cdot\mathbf{N})|\nabla\Phi|&=r\frac{\partial}{\partial r}\Phi\left(\frac{r}{r_0(\theta,\phi)}\right)\\&=\frac{r}{r_0(\theta,\phi)}\frac{\partial}{\partial\zeta}\Phi(\zeta)\\&=\zeta\frac{\partial}{\partial\zeta}\Phi(\zeta).\end{aligned} \tag{12}$$

This shows that the combination $(\mathbf{r}\cdot\mathbf{N})|\nabla\Phi|$ depends only on ζ, and so is constant over each smectic layer. We can therefore write

$$(\nabla\Phi)^2=p(\theta,\phi)\Delta(\zeta), \tag{13}$$

with

$$p(\theta,\phi)=\left[\frac{\mathbf{r}_0(\theta_0,\phi_0)\cdot\mathbf{N}(\theta_0,\phi_0)}{\mathbf{r}_0(\theta,\phi)\cdot\mathbf{N}(\theta,\phi)}\right]^2, \tag{14}$$

$$\Delta(\zeta)=A_N[\nabla\Phi]^2|_{\zeta,\theta_0,\phi_0}, \tag{15}$$

where (θ_0,ϕ_0) is a reference direction and A_N is a normalization constant which adjusts for differences between reference directions on different patches. The absolute value of A_N is unimportant, but its relative value on different surface patches must be chosen for a consistent definition of $\Delta(\zeta)$ across the entire smectic surface. Thus we have separated the angular dependence out of the volume integral of $\nabla\Phi$. The result is

$$F_{C\,patch}=\frac{1}{2}B\int d\zeta[\zeta^2\{I_0-2I_1\Delta(\zeta)+I_2\Delta^2(\zeta)\}], \tag{16}$$

where I_N are moments of the minimal surface shape,

$$I_N=\int d\Omega r_0^3(\theta,\phi)p^N(\theta,\phi).$$

Simple consideration shows that a similar separation occurs in regions with cylindrical symmetry, in which case $r=\zeta r_0(\phi)$ and $|\nabla\Phi|$ is independent of the local z coordinate. The equations are similar to the above. Numerical values were calculated with the aid of the SURFACE EVOLVER software package [15]. We minimize the total F_C by varying with respect to $\Delta(\zeta)$. The results are tabulated in Table I. The total compression energy had only a very weak dependence on the core size a_0 for $a_0\ll L$.

Calculations of the compression energy depend greatly on the particulars of the surface shape, so we cannot give an accurate approximate expression for F_C. In general, however, the total compression energy should increase rapidly with genus. Since all layers in this construction have the same topology, there must be just as many layers in the cylindrical regions, of radius $\langle R\rangle$, as there are in the minimal surface patch regions, which have typical radius of order $L/4$. As the genus increases, the number of cylindrical handles increases, as will the difference between $\langle R\rangle$ and $L/4$. This, in turn, will increase the overall compression energy.

For our proposed smectic structure to be stable against the uniform flat phase, the positive energy contributions from F_C, F_B, and $F_{\rm core}$ must be compensated by a large negative saddle splay energy. Since there is no chirality in our construction, the unit cell length can only arise as a result of the different scalings of these energies. We found that the scaling competition between the core and saddle splay energies was

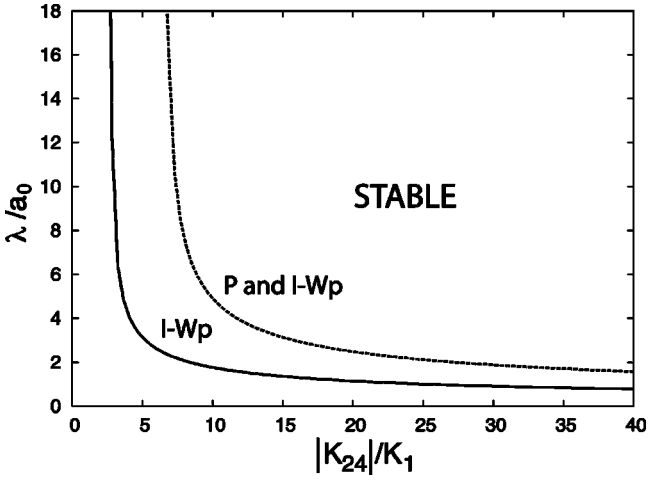

FIG. 4. Stability diagram for unit cells with $L=50a_0$. Our constructions based on P and I-Wp surfaces can be stabilized against flat layering in the regions of parameter space to the upper right of the, respectively, labeled lines. The quantity $\lambda\equiv\sqrt{K_1/B}$ is the penetration length.

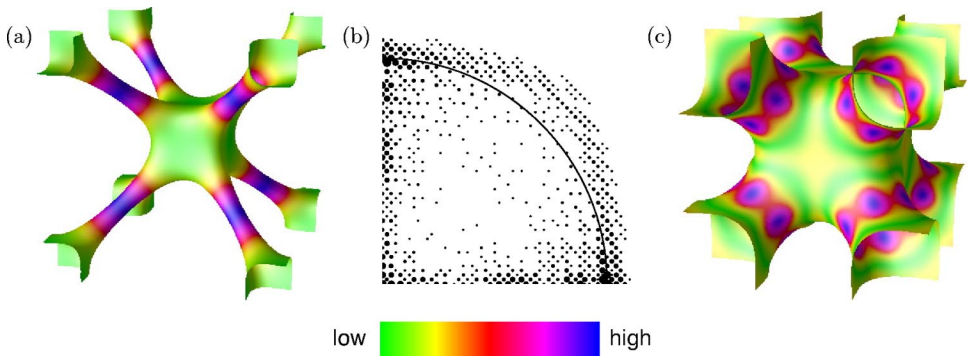

FIG. 5. (Color online) Numerical minimization results with parallel defect boundary conditions. Images (a) and (c) show two different smectic layers for a relaxed configuration of the I-Wp surface. Surface coloring is proportional to local curvature energy density, with blue and violet denoting the highest values. Plot (b) shows the strongest Fourier components in the $k_z=0$ plane for this smectic configuration.

capable of generating a length scale of $L=50a_0$, giving a preferred cell size for the P and I-Wp surfaces of the order of

$$N_P=\frac{L}{a_0}\approx\frac{12\pi|K_{24}|+[16/\pi-6]\varepsilon}{2\pi|K_{24}|-\varepsilon}, \tag{17}$$

$$N_{I\text{-}Wp}=\frac{L}{a_0}\approx\frac{72|K_{24}|-2.8\varepsilon}{7.6|K_{24}|-\varepsilon}. \tag{18}$$

We compare the total energy of the minimal surface smectics against that of uniform smectic configuration. Figure 4 shows the exact stability diagram of both the P and I-Wp surfaces, assuming a crystal unit cell length $L=50a_0$ to make contact with experiment. There are stable solutions of the P surface smectic for values of $|K_{24}|/K_1>6.5$ and for the I-Wp surface smectic for values of $|K_{24}|/K_1>2.7$.

B. Numerical minimization

In order to study elastic relaxation away from our simplified construction, we performed a numerical minimization of the smectic energetics of Eqs. (1) and (3) on a three-dimensional grid. The smectic field was represented by a single value of the phase Φ at each point on a 41 or 128 unit cubic grid with periodic boundary conditions. Discretized energy expressions were used to calculate the local values of compression, curvature, and saddle splay energy. We manually put line defects into our lattice which forced the P surface or I-Wp surface topology, similar to the analysis in Ref. [16]. The energy was then minimized by the conjugate-gradient method. Because of the troublesome nature of defining and allowing defects in such a phase field simulation, as well as the relatively small grid size, the numerical values in these simulations cannot be considered precise. However, study of the numerical minimal energy configurations are instructive for both validating and expanding upon our models.

We imposed parallel boundary conditions on the smectic field at the defect lines (in other words, the defect lines become surfaces of constant phase). This corresponds to our ''small-core'' construction. The results are pictured in Fig. 5. The shading indicates local bending energy density. For B/K_1 relatively small, the middle surface between inner and outer defect lattices is close to a minimal surface. For layers away from the middle surface, such as that pictured in Fig. 5(a), the curvature energy is concentrated around the cylindrical regions, while the remaining areas are close to minimal surfaces. Figure 5(b) shows the strong Fourier components in the $k_z=0$ plane for the I-Wp surface smectic. The numerically relaxed configurations for moderate values of $\lambda\equiv\sqrt{K_1/B}\approx 1$ and $L/a_0\approx 40$ layers per unit cell had a structure reminiscent of the experiments of Pansu *et al.* [6]: in their data they found that in an angular scan away from the maximum peaks the maximum intensity moved out to larger magnitudes in reciprocal space. We find this same off-peak increase for $|k_{max}(\theta,\phi)|$ for the relaxed configurations in this model.

For higher values of B/K_1, such as in Fig. 5(c), the smoothly curved regions of our construction start to become

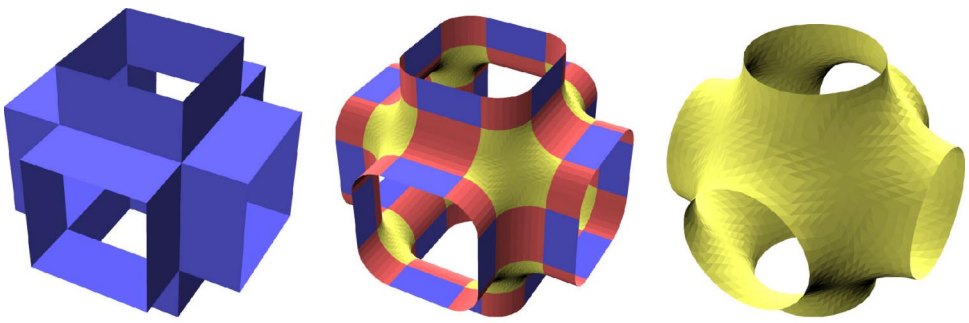

FIG. 6. (Color online) A one parameter model for curvature condensation to balance curvature and compression energies.

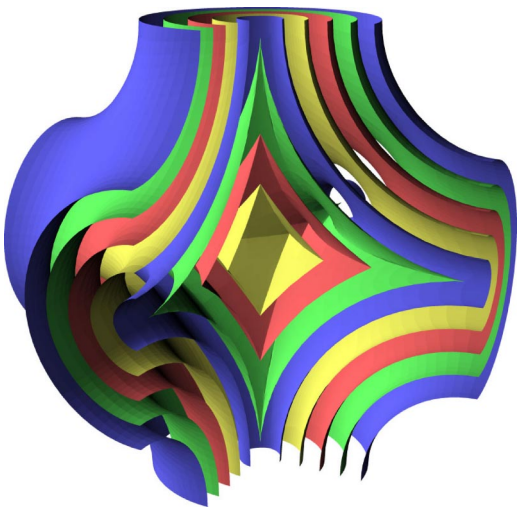

FIG. 7. (Color online) Construction of smectic blue phase based on uniform layer spacing of the Schwartz P surface. The image shows a cutaway of the layered structure inside the P surface.

faceted, with the curvature condensing onto discrete folds. This is not unlike the condensation of curvature found in crumpled elastic sheets [17]. Motivated by this apparent tradeoff between curvature and compression energies, we examined the model for relaxation pictured in Fig. 6, in which the regions of high curvature become more concentrated in space while the remaining overall surface becomes more polyhedral. This model has one continuous parameter $\chi \in [0,1]$ which interpolates between the minimal surface model at $\chi=1$ and a faceted surface with uniform layer spacing away from tilt-grain boundaries at $\chi=0$. In this model, we shrink patches of the minimal surface onto vertices of a polyhedron with the same symmetry. The patches are connected by cylindrical sections, and the remaining area is filled with flat facets. An expression for the compression energy of this structure, using our earlier techniques, is complicated, but numerical evaluation for the P surface found it was well approximated by a simple linear function of χ. The curvature energy is found by adding up the contributions of the cylindrical regions. We have ignored the complicated nonlinear effects at low χ, so our analysis is valid near $\chi=1$. The resulting combined compression and curvature energy density for the P surface smectic is

$$F_B+F_C=(4.32\times 10^{-2})\chi BL^3 + 6\pi K_1 L\left[\frac{1}{\chi}\ln(L/4\rho_c)+(4\rho_c/L-1)\right]. \quad (19)$$

Minimizing in χ gives

$$\chi=\sqrt{\frac{12\pi K_1 \ln(L/4\rho_c)}{(4.32\times 10^{-2})BL^2}}=0.94\frac{\lambda}{a_0}, \quad (20)$$

where the last equality is for $L=50a_0$. Since $\lambda \geqslant a_0$ and this treatment is only valid for $\chi \leqslant 1$, we see that curvature condensation will not happen for our small smectic repeat unit, but might occur for $L \gg 50a_0$.

IV. LARGE-CORE MODEL: CALCULATION OF CURVATURE ENERGIES USING WEIERSTRASS REPRESENTATION

A. Geometric construction

The large-core variant of our construction begins with a single continuous surface, then adds successive layers which are equally spaced along the original surface normals. As we showed in Sec. II, the continuation of uniform layer spacing will eventually lead to singularities. Figure 7 shows the results of this construction for the interior of a P surface section. The initial curvature singularities occurs on the nearly circular interface between unit cells of the P surface: essentially, the circular interface shrinks to a point, pinching off the connection between the interior layers and the outside of the unit cell. Any further layers within the pinched layer must be topologically like a sphere, with genus 0. Note that this layering scheme appears similar to the construction of constant mean curvature (CMC) surfaces [18] but is essentially different; there is no energetic preference for constant mean curvature and the CMC surfaces do not minimize the compression energy. We shall label the normal distance from the initial minimal surface to the last fully connected surface as a_{max}. Since the principal radii of curvature are equal and opposite for points on the minimal surface, the value of $|a_{max}|$ will be the same on both sides of the minimal surface. We call the region within the pinch-off surface, at distance greater than a_{max} from the minimal surface, the core region since our initial ordering is disrupted in this volume. Outside the core, the saddle splay energy per unit cell is $F_{SS}=16|K_{24}|(g-1)a_{max}$. The values of g and a_{max} for the P and I-Wp surfaces are given in Table II. Figures 2(a–c) show the surfaces defined by a_{max} for both minimal surfaces. Within the pictured surfaces, the continuation of our initial construction produces additional curvature singularities and lines of surface self-intersection. At the end of this section we justify a model for the core, which fills it with even layers joined by tilt-grain boundaries.

By insisting on uniform spacing away from the fiducial minimal surface, we determine the exact shape of all the layers outside the core with no free parameters. Clearly, the

TABLE II. Surface geometries and energies in the ''large-core'' construction for the P and I-Wp surfaces. The first column gives the generating function for the Weierstraß representation, followed by the maximum half-thickness of continuous layering, the curvature energy, saddle-splay energy, and grain-boundary core energy for this ansatz.

Surface	$R(\omega,\overline{\omega})$	a_{max} (L)	F_B (K_1L)	F_{SS} $(\lvert K_{24}\rvert L)$	F_{GB} $(K_1 a_0^{-1}L^2)$
P	$(1+14\omega^4+\omega^8)^{-1/2}$	0.232	12.2	−23.3	1.65
I-Wp	$(\omega^6-5\omega^4-5\omega^2+1)^{-2/3}$	0.150	14.7	−45.2	1.36

shape equations of all the layers can be obtained from that of the original surface if we know how all quantities evolve with normal displacement. The curvature evolution was derived in Sec. II. We can also map the area element of the initial surface to that on successive surfaces by $dA' = dA(1 + 2aH + a^2 K_G)$. This allows us to express the curvature component of the smectic free energy (3) as

$$F_B = 4K_1 \int_0^{a_{max}} da \int dA \frac{(H + aK_G)^2}{1 + 2aH + a^2 K_G}, \qquad (21)$$

where the area integral is taken over the center surface. In our case the area integral is over the minimal surface repeat cell and $H = 0$. We evaluated the surface integral in Eq. (21) analytically using the Weierstraß representation for the minimal surfaces [19,20], as described in Appendix B. Table II gives numerical values for the bending energy using Eq. (21) and the saddle-splay energies using the Gauss-Bonnet theorem and Eq. (2). In both cases the integration limit a_{max} corresponds to the value of a for which H' in Eq. (7) first diverges at some point on the surface. Thus, $a_{max} = (-K_G^{min})^{-1/2}$, with K_G^{min} the minimum (most negative) value of K_G on the minimal surface.

All that remains is to find the optimal way to fill the ''core'' volumes for $|a| > |a_{max}|$. The shape of these regions is shown in Figs. 2(a–c). In the core, the continuation of uniform layer spacing from the minimal surface leads to curvature singularities and layer self-intersections. However, as shown in Fig. 7, we can fill this volume with uniformly spaced domains of smectic order which intersect each other in tilt-grain boundaries. Within a domain, each point on a given layer is an equal normal distance away from some point on the initial minimal surface. Points on the grain boundaries between domains are an equal normal distance away from at least two different points on the minimal surface, so the grain boundaries occur where the uniform spacing used outside the core would cause layer self-intersection. We have no general principle of why the singularities in the core region are domain walls instead of, say, focal conic domains (such as you may find by developing a catenoid). For both the P and I-Wp surfaces uniform spacing leads to disclination walls, as it probably does for all but highly symmetric surfaces.

Thus, with the aim of avoiding layer compression, we choose this solution for the core structure, which should serve as an energetic upper bound. The energy of the core will arise from the regular curvature and saddle splay energies within the smectic domains, along with a surface energy at the grain boundaries and a separate line energy in the highly distorted regions where the grain boundaries meet. A conservative estimate of the energy of a tilt-grain boundary is $\approx K_1 a_0^{-1}$ per unit area [21] (assuming a melted wall of thickness a_0 at the defect plane). Numerically, the total area of grain-boundary walls per unit cell in this construction is $A = 1.65L^2$ for the P surface and $A = 1.36L^2$ for the I-Wp surface; the corresponding energies are given in Table II. The lines at the intersection of grain boundaries are located where the $+1$ and $+1/2$ disclinations were in the small-core model of Sec. III. Around these lines the director field varies so rapidly that the smectic order should melt completely, leaving a core of radius $\sim a_0$ and line tension ε. The mean curvature energy in the smectic domains is relatively small, since the shape of the innermost layers is mapped by Eq. (7) from the region around the umbilics (flat points) on the minimal surface. The inner layers are thus nearly flat. We found that the curvature energy was negligible by numerical evaluation.

The saddle-splay energy in the core merits special attention. Since the smectic layers in the core are not closed surfaces, our simple topological arguments do not apply. We could insist on connecting the surface sections together in a natural way across grain boundaries to obtain closed surfaces with the topology of a sphere. However, these closed surfaces are nearly polygonal, with all the Gaussian curvature concentrated at the vertices, or along the lines in three dimensions where the smectic order has melted. Thus, it is natural to assume that the smectic order parameter vanishes in these linelike cores, and the total saddle splay of the core is nearly zero. Of course, nematic order would likely persist inside the core. Since we are focussing here on the saddle splay associated only with the smectic order, i.e., the local Gaussian curvature, we have not considered the nematic saddle splay. These two contributions are distinct and adding the latter would be straightforward but would complicate the discussion.

The dominant free energy terms which determine the stability and preferred size of this construction are therefore the bend, saddle-splay, and grain-boundary energies. Minimizing these energies in a unit cell of length L gives

$$L = (|F_{SS}| - F_B)/(2F_{GB}). \qquad (22)$$

At this length the phase is stable against the standard, flat smectic when $|F_{SS}| > F_B$. Reading values from Table II, the minimum for the P surface structure occurs for $L = 7.06a_0(|K_{24}| - 0.523K_1)/K_1$, while that for the I-Wp occurs at $L = 16.6a_0(|K_{24}| - 0.325K_1)/K_1$. To compare with experiment we set $L = 50a_0$, where a_0 is the smectic layer spacing. This requires $|K_{24}|/K_1 = 6.6$ for the P surface or 2.6 for the I-Wp surface. Thus the I-Wp ansatz should be the stable phase at any value of K_{24}.

B. Numerical minimization

As before, we used conjugate-gradient minimization to explore the possible smectic configurations. In this case we relaxed the parallel boundary conditions, letting the interface of smectic field and defect line be arbitrary. The results are shown in Fig. 8. The core region resembles our ''large-core'' model, except that the defect walls have disappeared at the expense of greater overall compression. Locally, the core layers look like focal conics around the defect lines. This result undoubtedly points to configurations close to our model but with lower energy, and most likely stable for even lower values of $|K_{24}|/K_1$. Due to numerical difficulties, these phases could only be made stable for large values of $L/a_0 > 80$, so we could not compare configurations in the region of interest.

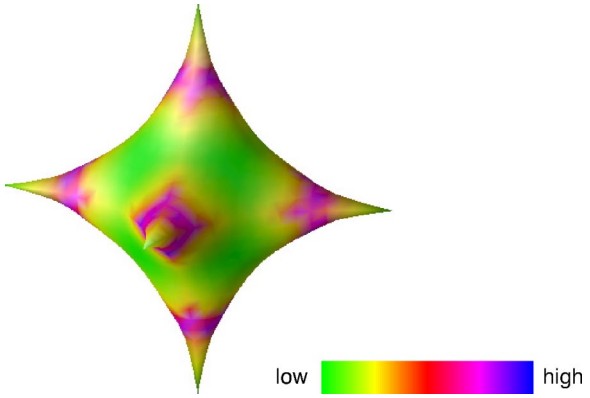

FIG. 8. (Color online) Numerical minimization results with arbitrary defect boundary conditions. The image shows the core region of a P surface smectic.

V. COMPARISON TO SPECTROSCOPIC DATA

Pansu *et al.* [5–7] found through x-ray diffraction that the cubic $BP_{SmA}1$ phase showed the strongest diffraction along three mutually orthogonal axes. They also found that the peak wavelength of diffraction decreased away from these special directions. In order to compare our model to their data, we have calculated the expected scattering from a smectic blue phase built by our large-core construction. Figure 9 shows the *k*-space location of the strongest Fourier peaks for both a P surface smectic and an I-Wp surface smectic. In each case, we sampled the smectic phase on a cubic grid with 128 points per side. We took the smectic phase to be $2\pi\times 37\times x_n/L$, where x_n is the distance of the sample point normal to the minimal surface. We chose this number of layers to avoid any commensuration effects. Because there are many layers, this was numerically challenging and a higher precision study is needed, such as the study of scattering from triply periodic minimal surfaces by Garstecki and Hołyst [22].

For both structures, and we expect for general minimal surface smectics, the Fourier peaks were strongest along the umbilics of the minimal surfaces, i.e., normal to the points at which the surfaces are flat. The Fourier peaks of the I-Wp structure are a clear match to the observed x-ray diffraction of $BP_{SmA}1$. However, as Fig. 9(c) shows, there is no clear deviation in diffraction maximum wavelength as a function of angle (Pansu *et al.* reported a 7% deviation over 25° angle). This indicates the need for further refinement to our model if it is to explain the current data exactly. The discrepancy in off-peak behavior between our simulations and real data could arise from some relaxation of our proposed structure to better accommodate the competing energies. As we noted in Sec. III B, the numerical relaxation of the I-Wp smectic with parallel (small-core) boundary conditions does produce the correct off-peak behavior for the diffraction maxima.

VI. CONCLUSION

We have presented a model for smectic blue phases which is stable for physically realizable values of K_{24} and penetration length $\lambda\equiv\sqrt{K_1/B}$. This work refines that of our previous paper [10] and gives further weight to our proposed organizing principle of smectics built on minimal surfaces. Unlike the traditional blue phases, our model does not rely on molecular chirality. It would be interesting to add chirality into this model to see how the length scale alters the equilibrium structures. We have also addressed the broader question of geometrical frustration between Gaussian curvature and smectic order. Our computed structure factor matches the scattering from the $Sm_{BP}1$ phase and so we remain optimistic that our construction could be verified, perhaps through freeze fracture.

ACKNOWLEDGMENTS

We thank T. C. Lubensky, B. Pansu, and J. P. Sethna for fruitful discussions. This work was supported by NSF Grant Nos. INT99-10017 and DMR01-29804, the Donors of the Petroleum Research Fund Administered by the American Chemical Society, and a gift from L. J. Bernstein.

APPENDIX A: ALTERNATE DERIVATION OF CURVATURE EVOLUTION; LAYERING AND CURVATURE FRUSTRATION IN CURVED SPACE

The first result in Eq. (5) also follows by considering the derivative of the mean curvature along the layer normal:

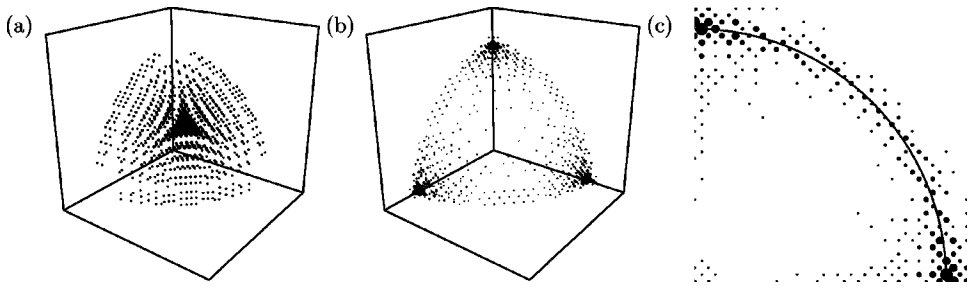

FIG. 9. Discrete Fourier transform of proposed smectic structures. Plot (a) is for the P surfaced based construction, (b) and (c) are for the I-Wp construction. Plots (a) and (b) show the largest Fourier components in the positive coordinate octant of *k* space. Plot (c) shows the largest Fourier components in the positive coordinate quadrant of the $k_z=0$ plane. Point size is proportional to the Fourier coefficient at that $\vec{k}$.

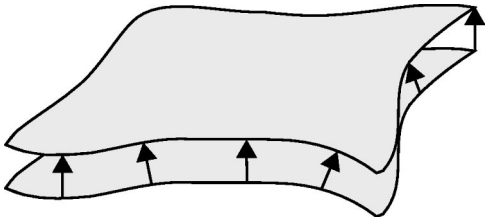

FIG. 10. One patch being uniformly translated along its normal. The top and bottom surfaces along with the perpendicular surfaces generated by the normals at the boundaries makes an integration volume V.

$$\frac{\partial H}{\partial a}=(\mathbf{N}\cdot\boldsymbol{\nabla})\left[\frac{1}{2}\boldsymbol{\nabla}\cdot\mathbf{N}\right]=\frac{1}{2}\boldsymbol{\nabla}\cdot[\mathbf{N}(\boldsymbol{\nabla}\cdot\mathbf{N})]-\frac{1}{2}(\boldsymbol{\nabla}\cdot\mathbf{N})^2. \tag{A1}$$

When the layers are built by developing surfaces parallel to a fiducial surface, the layer normals do not change—in other words, since we are translating the surface parallel to $\mathbf{N}$, we must have $(\mathbf{N}\cdot\boldsymbol{\nabla})\mathbf{N}=0$ [23]. Adding this term to Eq. (A1) we have

$$\frac{\partial H}{\partial a}=\frac{1}{2}\boldsymbol{\nabla}\cdot[\mathbf{N}(\boldsymbol{\nabla}\cdot\mathbf{N})-(\mathbf{N}\cdot\boldsymbol{\nabla})\mathbf{N}]-\frac{1}{2}(\boldsymbol{\nabla}\cdot\mathbf{N})^2=K_G-2H^2. \tag{A2}$$

Similarly, consider a patch on one layer and the corresponding patch on a uniformly translated surface as shown in Fig. 10. Because the principle directions of the two surfaces are unchanged, the geodesic curvature of the corresponding boundaries are identical. It follows from the Gauss-Bonnet theorem that $\int_{M_{1,2}}K_G dA$ is the same on the two patches. Thus, over the volume V swept out by making the translated patch (shown in Fig. 10), $\int_V K_G\mathbf{N}\cdot d\mathbf{A}=0$. Therefore, $\boldsymbol{\nabla}\cdot(K_G\mathbf{N})=0$ and

$$0=\mathbf{N}\cdot\boldsymbol{\nabla}K_G+K_G\boldsymbol{\nabla}\cdot\mathbf{N},$$

$$0=\frac{\partial K_G}{\partial a}+2K_G H. \tag{A3}$$

The intrinsic frustration between curvature and uniform layer spacing can be relieved by considering layered systems in curved space, just as double twist in the classical blue phases can fill the surface of the three-dimensional sphere without defects [24]. It is straightforward to see this using the derivations above. In curved space, we simply replace derivatives with *covariant* derivatives, so that $\boldsymbol{\nabla}\rightarrow\mathbf{D}$, where $\mathbf{D}$ is the covariant derivative [25]. The mean curvature is $H=\frac{1}{2}D_i N^i$ and is essentially unchanged. However, the relation between Gaussian curvature and saddle splay is more subtle. Recall that in flat space, the coefficients of the two terms in the saddle splay are constrained so that the saddle splay only depends on first derivatives of $\mathbf{N}$. We shall see that this is spoiled in curved space. We have

$$\begin{aligned}\mathbf{D}\cdot[(\mathbf{N}\cdot\mathbf{D})\mathbf{N}-\mathbf{N}(\mathbf{D}\cdot\mathbf{N})]&=D_i[N^jD_jN^i-N^iD_jN^j]\\&=(D_iN^jD_jN^i-D_iN^iD_jN^j)\\&\quad+N^j[D_i,D_j]N_i.\end{aligned} \tag{A4}$$

The first term in Eq. (A4) is $-2K_G$, a factor times the Gaussian curvature. Note that in flat space, the covariant derivatives become simple derivatives and commute. In curved space this is no longer true and the commutator term is just R_{NN}, the component of the Ricci tensor in the normal-normal direction. The evolution equation for K_G is unchanged since Stoke's theorem (properly modified) holds in curved space. Thus in curved space we have

$$\frac{\partial K_G}{\partial a}=-2K_G H,$$

$$\frac{\partial H}{\partial a}=K_G-2H^2-\frac{1}{2}R_{NN}. \tag{A5}$$

Thus we can have uniformly spaced layers with $H=0$ and K_G constant (K_G may vary in the layer, but will not change from layer to layer) if we embed the smectic in a space with $R_{NN}=2K_G$. Since we are considering surfaces with $K_G<0$, this suggests a space with negative curvature.

To see this, we consider a special coordinate system in a three-dimensional layered structure. For unbroken layers we can uniquely define the continuous variable Φ which labels the layers. Furthermore, we can use Φ as a local coordinate to define a coordinate basis in which one basis vector e_3 is dual to the directional derivative in Φ, and the other basis vectors e_1 and e_2 lie in planes of constant Φ. This coordinate system is known as Gaussian normal coordinates [25]. Furthermore, for uniform layer spacing the measurement of distance along e_3 cannot depend on coordinates 1 and 2. This, plus the orthogonality of e_3 lets us scale our coordinates such that $g_{3i}=e_3\cdot e_i=\delta_{3i}$.

Since we are using a coordinate basis, the covariant derivative is defined with the typical connection coefficients $\Gamma^i{}_{jk}$. Elementary considerations relate the connection coefficients to the extrinsic curvature tensors of the layers taken as two sheets

$$\kappa_{ij}=\Gamma_{3ij}=-\Gamma_{i3j}=-\Gamma_{j3i}\quad\text{for}\quad i,j\neq 3,$$

$$\Gamma_{i33}=\Gamma_{3i3}=\Gamma_{33i}=0. \tag{A6}$$

Laborious but autonomic calculations show that the Ricci scalar $R=2R_{NN}$ and so the space has negative scalar curvature. This is not surprising: in the classical blue phases the saddle splay elastic constant needed to be *positive*, favoring positive Gaussian curvature, and the resulting structure could be defect-free in positively curved space. We have merely ''flipped the signs'' on the last sentence. Further work on flattening the hyperbolic space into $\mathbb{R}^3$ would be interesting and may shed light on the preferred lattices.

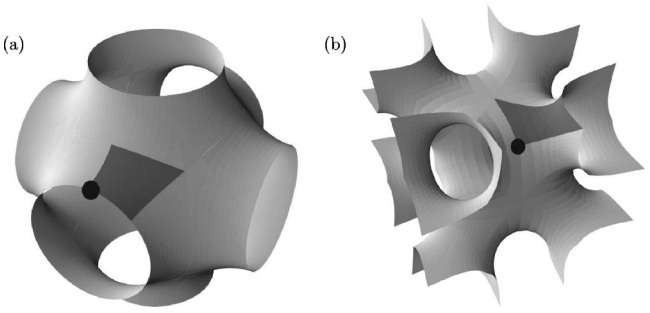

FIG. 11. Weierstraß representation of the P surface, (a), and the I-Wp surface, (b). The shaded region in each is 1/48 part of the pictured surface repeat unit and contains all the symmetry of the entire surface. The points represent the location of $\omega=0$ for the Weierstraß mappings given in Table II.

APPENDIX B: WEIERSTRAß REPRESENTATION OF MINIMAL SURFACE

The Weierstraß representation of minimal surfaces relies on the fact that there is locally a one to one mapping from a minimal surface onto the unit sphere via the surface normal [19]. The unit sphere can, in turn, be mapped onto the complex plane by stereographic projection, with the plane passing through the equator of the sphere. The latter mapping gives the components of the surface normal in terms of the complex variable $\omega=\sigma+i\tau$ as

$$N_1=\frac{2\,\mathrm{Re}\,\omega}{1+|\omega|^2},\quad N_2=\frac{2\,\mathrm{Im}\,\omega}{1+|\omega|^2},\quad N_3=\frac{1-|\omega|^2}{1+|\omega|^2}. \tag{B1}$$

The reverse mapping between the complex plane and the minimal surface itself can be expressed via a single generating function $R(\omega,\bar{\omega})$. In terms of $R(\omega,\bar{\omega})$, displacements on the minimal surface are

$$dx^1=\mathrm{Re}[(1-\omega^2)R(\omega,\bar{\omega})d\omega],$$
$$dx^2=-\mathrm{Im}[(1+\omega^2)R(\omega,\bar{\omega})d\omega],$$
$$dx^3=-2\,\mathrm{Re}[\omega R(\omega,\bar{\omega})d\omega]. \tag{B2}$$

The relative coordinates of points on the surface can be found by integrating Eq. (B2).

To complete our reparametrization of Eq. (21) in terms of ω, we quote expressions for other quantities of interest on the surface [19,20]:

$$dA=|R(\omega,\bar{\omega})|^2(1+|\omega|^2)^2d\sigma d\tau,$$
$$K_G=-4|R(\omega,\bar{\omega})|^{-2}(1+|\omega|^2)^{-4}. \tag{B3}$$

The Weierstraß representations for the surfaces we consider are given in Table II. For the P surface, $\omega=0$ ($z=-1$ on the unit sphere) corresponds to the point indicated in Fig. 11(a). The entire shaded region in Fig. 11(a), which is 1/48 of the P surface repeat cell, maps to the region on the unit sphere bounded by the intersection of the sphere with the planes $x=0$, $y=0$, $z=-x$, and $z=-y$. For the I-Wp surface, the position of $\omega=0$ is shown in Fig. 11(b). The shaded region is again 1/48 of the I-Wp repeat cell and corresponds to the region on the unit sphere bounded by the planes $x=0$, $y=0$, $z=x$, and $z=\sqrt{2}y-x$.

[1] Z. Kutnjak, C.W. Garland, J.L. Passmore, and P.J. Collings, Phys. Rev. Lett. **74**, 4859 (1995); J.B. Becker and P.J. Collings, Mol. Cryst. Liq. Cryst. **265**, 163 (1995).
[2] H.-S. Kitzerow and P.P. Crooker, Phys. Rev. Lett. **67**, 2151 (1991); H.M. Hornreich, *ibid.* **67**, 2155 (1991).
[3] B. Pansu, M.-H. Li, and H.T. Nguyen, J. Phys. II **7**, 751 (1997).
[4] E. Grelet, B. Pansu, M.-H. Li, and H.T. Nguyen, Phys. Rev. E **65**, 050701(R) (2002).
[5] E. Grelet, B. Pansu, M.-H. Li, and H.T. Nguyen, Phys. Rev. Lett. **86**, 3791 (2001).
[6] B. Pansu, E. Grelet, M.-H. Li, and H.T. Nguyen, Phys. Rev. E **62**, 658 (2000).
[7] E. Grelet, B. Pansu, and H.T. Nguyen, Phys. Rev. E **64**, 010703(R) (2001).
[8] R.D. Kamien, J. Phys. II **7**, 743 (1997).
[9] S. Meiboom, J.P. Sethna, P.W. Anderson, and W.F. Brinkman, Phys. Rev. Lett. **46**, 1216 (1981).
[10] B.A. DiDonna and R.D. Kamien, Phys. Rev. Lett. **89**, 215504 (2002).
[11] R.D. Kamien, Rev. Mod. Phys. **74**, 953 (2002).
[12] When $g=0$ the unit cell must have the topology of a sphere and cannot have any handles or holes to allow it to connect to the neighboring unit cells.
[13] R. Capovilla and J. Guven, J. Phys. A **35**, 6233 (2002).
[14] The Scientific Graphics Project, http://www.msri.org/publications/sgp/SGP/indexc.html
[15] K. Brakke, Exp. Math. **1**, 141 (1992).
[16] W. Gózdz and R. Hołyst, Phys. Rev. E **54**, 5012 (1996).
[17] B.A. DiDonna, Phys. Rev. E **66**, 016601 (2002).
[18] D. Anderson, H. Davis, L. Scriven, and J.C.C. Nitsche, Adv. Chem. Phys. **77**, 337 (1990).
[19] J.C.C. Nitsche, *Vorlesungen über Minimalflächen* (Springer-Verlag, Berlin, 1975); J.C.C. Nitsche, *Lectures on Minimal Surfaces* (Cambridge University Press, Cambridge, 1989) (translated by J.M. Feinberg).
[20] B. Pansu and E. Dubois-Violette, Europhys. Lett. **10**, 43 (1989).
[21] M. Kléman, *Points, Lines and Walls* (Wiley, New York, 1983).
[22] P. Garstecki and R. Hołyst, Phys. Rev. E **64**, 021501 (2001).
[23] J.P. Sethna and M. Kléman, Phys. Rev. A **26**, 3037 (1982).
[24] J.P. Sethna, D.C. Wright, and N.D. Mermin, Phys. Rev. Lett. **51**, 467 (1983).
[25] C.W. Misner, K.S. Thorne, and J.A. Wheeler, *Gravitation* (Freeman, New York, 1973).